Optical Materials 99 (2020) 109553

Contents lists available at ScienceDirect

Optical Materials

journal homepage: http://www.elsevier.com/locate/optmat

Intrinsic electronic excitations and impurity luminescent centres in $NaMgF_3$ and MgF_2 doped with Yb^{2+}

Rosa B. Hughes-Currie [a,b], Konstantin V. Ivanovskikh [c], Jon-Paul R. Wells [a,b,*], Michael F. Reid [a,b], Andries Meijerink [d]

[a] School of Physical and Chemical Sciences, University of Canterbury, PB 4800, Christchurch, 8140, New Zealand
[b] Dodd-Walls Centre for Photonic and Quantum Technologies, New Zealand
[c] Experimental Physics Department, Ural Federal University, 19 Mira St., Ekaterinburg, 620002, Russia
[d] Debye Institute for NanoMaterials Science, Utrecht University, P.O. Box 80 000, 3508, TA Utrecht, the Netherlands

ARTICLE INFO

Keywords:
Self-trapped exciton
Impurity-trapped exciton
Lanthanide
Ytterbium
NaMgF3
MgF2
Synchrotron radiation
VUV spectroscopy

ABSTRACT

The relaxation pathways of states in the energy region of the fundamental absorption of $NaMgF_3$:Yb^{2+} and MgF_2:Yb^{2+} are investigated using time-resolved vacuum ultraviolet spectroscopy. For $NaMgF_3$:Yb^{2+}, excitation into intrinsic free exciton states or above the band gap results in emission features associated with self-trapped excitons and impurity-trapped excitons. Excitation into host-related states of MgF_2:Yb^{2+} similarly exhibits self-trapped exciton emission as well as emission from Yb^{2+} $4f^{13}5d$ states. The excitation features related to Yb^{2+} $4f^{14}\rightarrow4f^{13}5d$ transitions are interpreted using semi-empirical crystal field models. For both materials, the interplay between intrinsic distortions and Yb impurity centres, as the excitation wavelength and sample temperature are varied, is presented and analysed.

1. Introduction

Electronic transitions in lanthanide doped wide bandgap materials include formation and relaxation of *e-h* pairs, excitonic processes, charge exchange or charge transfer transitions, and transitions within a localized impurity ion. Understanding the interplay between the above mentioned fundamental processes may lead to better engineered materials for applications as scintillators or phosphors, in lighting and dosimetry. While the processes related to the relaxation of primary electronic excitations are similar enough in many types of optical wide bandgap materials, the following steps may demonstrate varieties dependent on electronic structure of a particular impurity ion and its interaction with the host. Charge exchange processes occurring between the lanthanide impurity and the host conduction band (CB) may result from photoionization of electron in an excited 5d state through electron-to-donor transitions of the impurity. Ionisation of 5d electron and its delocalization over the next-neighbour metal-ions (so called delocalized Rydberg states) may lead to the formation of impurity-trapped exciton (ITE) where hole moiety remains localized on the impurity. In some cases, the ITE may decay radioactively that results in broad emission band with large Stokes shift. Obviously, formation of ITE is a quenching process that prevents $4f^{13}5d\rightarrow4f^{14}$ radiative decay. Such process are often referred to 'anomalous emission' and are observed in fluoride crystals doped with Yb^{2+}, and in some cases Eu^{2+}.

The materials CaF_2, $NaMgF_3$ and MgF_2 doped with Yb^{2+} have usually been considered as good candidates for studying the ITE related phenomena due to their wide band gaps [1–4]. Previous work on the VUV spectroscopy of CaF_2:Yb^{2+} has shown emission due to both impurity-trapped exciton (ITE) and self-trapped exciton (STE) states with evidence of energy transfer between them [5]. We note that the ITE model itself was recently shown to not fully describe all observations related to anomalous emission in Yb-doped CaF_2 and SrF_2. A more recent model suggests that this emission is associated with an intervalence charge transfer process associated with the presence of Yb^{2+} - Yb^{3+} mixed valence pairs [6–10]. These results do not invalidate the ITE model but rather point to complexity of relaxation processes followed $4f^{14}\rightarrow4f^{13}5d$ excitation Yb^{2+} ion in fluorites. In this connection it is important to expand our understanding of the spectroscopy and dynamics of Yb^{2+} $4f^{13}5d$ excited states in the wider fluoride family. In this work, we focus on time-resolved VUV spectroscopic study of $NaMgF_3$:Yb and MgF_2:Yb single crystals and compare the results to that previously published for CaF_2:Yb^{2+}.

* Corresponding author. School of Physical and Chemical Sciences, University of Canterbury, PB 4800, Christchurch, 8140, New Zealand.
E-mail address: jon-paul.wells@canterbury.ac.nz (J.-P.R. Wells).

https://doi.org/10.1016/j.optmat.2019.109553
Received 13 November 2019; Accepted 15 November 2019
Available online 21 November 2019
0925-3467/© 2019 Elsevier B.V. All rights reserved.

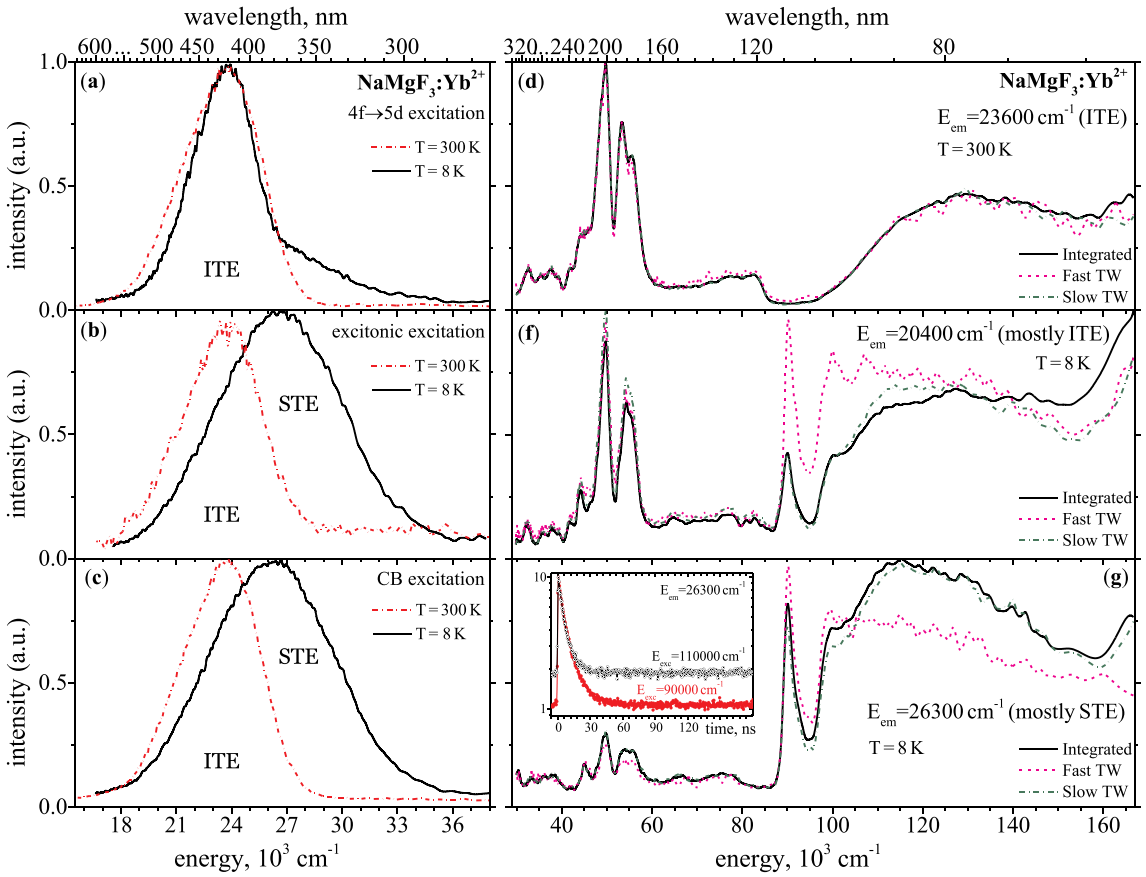

Fig. 1. $NaMgF_3:Yb^{2+}$. Emission spectra (left panels) recorded in time-integrated mode at T = 8K and T = 300 K upon 4f-5d excitation near 54000 cm^{-1} (a), excitation into free exciton formation peak at 90000 cm^{-1} and 87000 cm^{-1} at T = 8K and T = 300 K, respectively (b) and above the band gap at 117700 cm^{-1}. Excitation spectra (right panels) in time-integrated and time-resolved mode recorded monitoring the ITE emission near 23500 cm^{-1} (d) and 20400 cm^{-1} (f) at T = 300 K and T = 8K, respectively, and the STE emission near 26300 cm^{-1} T = 8K. Insert in panel (g) shows STE emission decay kinetics recorded upon excitation into free exciton formation peak and above the band gap. See more details on the graphs.

$NaMgF_3$ is a technologically important material having both mechanical and optical properties which make it a desirable host material for dosimetry applications, in particular. Optically stimulated luminescence (OSL) dosimetry measurements have been performed on $NaMgF_3$ doped with divalent europium [11] and trivalent cerium [12]. Finding new materials for applications such as OSL dosimetry is aided by greater understanding of the nature of the phenomena which lead to luminescence in the materials. The broad band emission observed when Yb^{2+} ions in $NaMgF_3$:Yb are excited with UV radiation into its $4f^{13}5d$ excited configuration is currently accepted to be associated with radiative relaxation from an ITE state [13]. ITEs are formed when a 5d electron becomes delocalized over surrounding cations; effectively - $Yb^{3+} + e^-$. UV excitation studies of $NaMgF_3:Yb^{2+}$ show two overlapping emission peaks associated with ITEs in two different charge-compensation arrangements [13,14].

Ultraviolet excitation of MgF_2:Yb also yields a broad visible emission band which has been previously interpreted as ITE emission [15] however recent studies have suggested this to be associated with a regular Yb^{2+} $4f^{13}5d \rightarrow 4f^{14}$ transition. MgF_2:Yb differs from both CaF_2:Yb and $NaMgF_3$:Yb in that the lowest component of the Yb^{2+} $4f^{13}5d^1$ excited state sits well below the conduction band. Dorenbos (2003) [16] suggested the emission from MgF_2:Yb deviated from where it would sit in comparison to $MgF_2:Eu^{2+}$ emission by $\Delta D = -0.26$ eV (2100 cm^{-1}), so it was possible that the emission should be classified as "anomalous" and correspond to ITE recombination. In a more recent study, Senanayake [17,18] utilised a UV-IR transient photoluminescence enhancement technique to investigate MgF_2:Yb observing electron trap liberation but no evidence of intra-excitonic transitions. It was concluded that the emission originated from a $4f^{13}5d \rightarrow 4f^{14}$ transition. Comparing the emission behaviour of MgF_2:Yb with alkaline earth fluoride hosts which exhibit exciton emission is useful in characterising the difference between emission originating in excitonic and intrinsic transitions and investigating the environmental factors which cause excitons form and decay radiatively.

When alkali earth halides are excited with vacuum ultraviolet radiation into free exciton states, the free excitons self-trap and radiatively recombine producing a broad visible self-trapped exciton (STE) emission band [19]. This work shows the dynamics of relaxation from host electronic states to STE, ITE and 5d Yb states.

2. Experimental

The $NaMgF_3$:Yb and MgF_2:Yb crystals used in this work contained 0.6 mol% of ytterbium and were grown using the Bridgman-Stockbarger technique in a reducing atmosphere. As such, they generally contain a mixture of ions having the divalent and trivalent ionisation states [20]. Absorption spectra were measured using a Cary 6000i spectrophotometer equipped with a temperature controlled, closed cycle cryostat system. The time-resolved VUV spectroscopic measurements were carried out using the SUPERLUMI facility at HASYLAB of DESY (Hamburg, Germany) with synchrotron radiation (SR) from the DORIS III storage ring [21]. The as-grown crystals were cleaved before mounting to the sample holder. A 2 m monochromator in McPherson mounting with a resolution of 3.2 Å was used for measurements of excitation spectra in the range of 30 000–170 000 cm^{-1}. The detection of the luminescence was done with a 0.3 m ARC SpectraPro-308i monochromator equipped

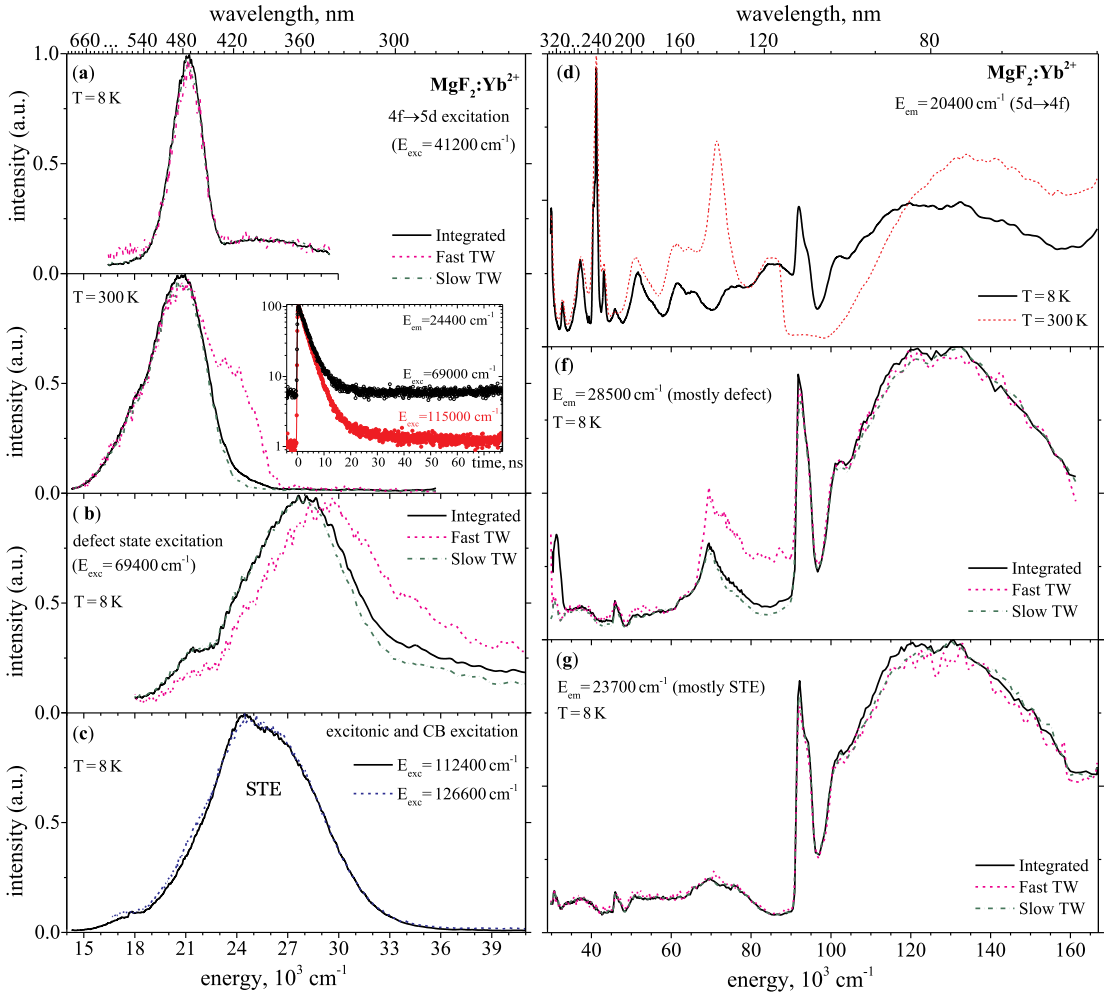

Fig. 2. $MgF_2:Yb^{2+}$. Emission spectra (left panel) recorded in time-integrated and time-resolved mode upon 4f-5d excitation near 41200 cm^{-1} (a), within transparency range in presence of 4f-5d and defect absorption at 61300 cm^{-1} (b), near defect absorption state at 69400 cm^{-1} (c), and into free exciton formation peak at 112400 cm^{-1} and above band gap at 126600 cm^{-1} (d). Excitation spectra (right panel) were recorded in time-integrated mode for Yb^{2+} 5d-4f emission (f), defect emission near 28500 cm^{-1} at T = 8 K (f) and STE emission monitored at 23 700 cm^{-1} at T = 8 K (g).

with a high-speed R3809U–50S (Hamamatsu) microchannel plate (MCP) detector. The time-integrated spectra were recorded by counting the emission signal within the whole time period of 480 ns available between SR pulses at a reduced (2) bunch mode (BM) of the storage ring. The time-resolved spectra were recorded within two time windows (TWs): 4–30 ns (fast time gate) and 248–420 ns (slow time gate) relative to the beginning of the SR pulse. The measurements were performed in the temperature range of 8–300 K in an ultra-high-vacuum chamber ($\sim 10^{-9}$ mbar). The excitation spectra were corrected for the wavelength-dependent variation of the SR intensity using a sodium salicylate signal. A background signal corresponding to the dark count of the MCP detector was subtracted from the original spectra and decay curves.

3. Results

3.1. Excitation and fluorescence of $NaMgF_3:Yb^{2+}$

Fig. 1 shows the $NaMgF_3:Yb^{2+}$ emission spectra recorded in time-integrated mode (left panel) and excitation spectra recorded in both time-integrated and time-resolved modes (right panel) at T = 8 K and T = 300 K. Upon excitation into the $4f^{13}5d$ states of Yb^{2+} at 41200 cm^{-1}, emission from the ITE is observed as an approximately Gaussian shaped emission band at 23800 cm^{-1} with a FWHM of 4210 cm^{-1} and 5020 cm^{-1} at T = 8 K and T = 300 K, respectively. The ITE is also observed upon excitation into the host (excitonic and CB) states at T = 300 K. For low temperatures, the ITE emission band is obscured by the intense STE emission band (Fig. 1-b, -c). The STE emission is a broad (FWHM ~ 4210 cm^{-1}) band centred near 26600 cm^{-1} and can only be excited via the formation of free excitons or upon higher energy excitation that corresponds to the generation of separated electron-hole pairs. At T = 300 K, the STE emission is quenched and emission spectra of $NaMgF_3:Yb^{2+}$ recorded upon host excitation, reflect ITE emission only. We note that the emission spectra recorded within fast and slow TWs do not reveal any noticeable deviations from those recorded in time-integrated mode and are not shown for brevity.

The excitation spectra recorded monitoring ITE emission at T = 8 K and T = 300 K demonstrate intense features in the energy range $E_{exc}<60000$ cm^{-1} which are connected to 4f-5d transitions (Fig. 1, d, f). The peak at 90 000 cm^{-1} observed in the low-temperature excitation spectrum (Fig. 1f and g) is the free exciton peak which has been reported in reflectance measurements [22]. The presence of the free exciton peak in the excitation spectrum of ITE emission provides direct evidence of energy transfer between intrinsic excitons and Yb^{2+}. The most likely

pathway from the formation of free excitons to ITE emission is the formation of STEs and energy transfer from the STEs to the Yb ions. Energy transfer from STEs to luminescent centres has been shown in other materials [23,24] including $CaF_2:Yb^{2+}$ [5].

The absence of the free exciton peak in the 300 K excitation spectrum recorded monitoring the ITE emission may be explained by thermally induced non-radiative relaxation of STE [25] and surface losses [23,26,27]. When the sample is excited above 95 000 cm^{-1} the relative intensity of the ITE emission increases. This emission increase suggests that there is also a pathway for host-to-impurity energy transfer involving relaxation of primary *e-h* pairs. We note that the relative intensity of the 8K excitation spectrum of the ITE in the range corresponding to direct formation of *e-h* pairs is almost double that at the excitonic peak. This is a manifestation of surface quenching where excitons with low kinetic energy are directly created with photons near 92 000 cm^{-1} resulting in a low intensity excitonic peak. The efficient energy transfer from *e-h* pairs to Yb^{2+} will be discussed below, along with results obtained for $MgF_2:Yb^{3+}$.

In the range of 128000–156000 cm^{-1} the ITE emission excitation spectra recorded at both T = 8 K and T = 300 K demonstrate a slight decrease of the quantum yield that is likely connected with migration losses due to increased escape during the thermalization stage [26,27]. A similar effect, over a wider energy range, is observed in the excitation spectrum of the STE emission.

The 8 K excitation spectra exhibit significant enhancement of the fast TW signal around the free excitonic peak. The insert in Fig. 1-g shows the emission decay curves recorded monitoring the STE emission band maximum upon excitation into the free exciton peak and above the band gap. The decay curves have a fast component with a time constant of 9 ns and a much slower decay component (tens of microseconds or even longer). The long-time decay component is present as a constant level (piling) due to overlay of the emission decay pulses excited by the continuous sequence of excitation pulses arriving with a high repetition rate (see Ref. [28] for details). The presence of a fast decaying component in the STE emission of $NaMgF_3$ was first documented in Ref. [29] and assigned to relaxation of the σ (singlet) component of the STE.

3.2. Excitation and fluorescence of $MgF_2:Yb^{2+}$

Fig. 2 presents the time-integrated and time-resolved emission spectra as well as the excitation spectra of $MgF_2:Yb^{2+}$ recorded for sample temperatures of T = 8 K and T = 300 K. When $MgF_2:Yb^{2+}$ is excited into the 5d states at E_{exc} = 41200 cm^{-1}, the 8 K emission spectrum is dominated by a relatively broad Pekarian shape d emission band centred at 21130 cm^{-1} with a FWHM = 2160 cm^{-1}. This emission feature has been previously ascribed to regular $4f^{13}5d \rightarrow f^{14}$ emission of the Yb^{2+} ion [17]. When the temperature is raised to 300K, the emission band slightly red shifts approximately 500 cm^{-1} and broadens by a factor of two (FWHM ~ 3940 cm^{-1}). The emission is dominated by the signal collected in the slow TW at any measured temperature. At temperatures above 200 K, we observe a weak emission band centred around 23 400 cm^{-1} that is excited both upon excitation within the transparency range and for direct host excitation. This signal is most pronounced within the fast TW spectrum (Fig. 2-a, lower panel). The insert in Fig. 2-a shows the luminescence decay profiles recorded monitoring the fast emission upon excitation at 69 000 and 115 000 cm^{-1} for T = 300K. The fast component in the decay profiles has a decay constant of 3.8 ns. The nature of the fast emission band is not well understood and requires further study that is beyond the scope of this paper. We note, however, that the spectral properties of the fast emission remain those documented for the emission of M-centres in MgF_2 [30].

The emission spectrum of $MgF_2:Yb^{2+}$ at T = 8 K demonstrates a noticeable dependence on excitation energy (i.e. the 'optical frequency' at which excitation occurs). Apart from the above mentioned Yb^{2+} $4f^{13}5d \rightarrow f^{14}$ emission, we observe a broad emission band centred near 27800 cm^{-1} (FWHM ~ 7870 cm^{-1}) of quite low intensity excited in the transparency range (Fig. 2-b) and emission at 25200 cm^{-1} (FWHM ~ 7320 cm^{-1}) due to radiative recombination of MgF_2 STEs from their triplet state (Fig. 2-c) [31]. The band at 27800 cm^{-1} is tentatively assigned to defect emission. The dip near 22100 cm^{-1} at the low energy side of this band results from reabsorption of the emission by Yb^{2+} ($4f^{14} \rightarrow 4f^{13}5d$ - see the experimental and simulated absorption spectra in Fig. 4). We note that upon host excitation at T = 8 K the $MgF_2:Yb^{2+}$ emission spectrum is dominated by the STE band that obscures the Yb^{2+} and the defect emission features.

The excitation spectra recorded monitoring Yb^{2+} $4f^{13}5d \rightarrow 4f^{14}$ emission at T = 8 K and T = 300 K are dominated by features related to $4f^{14} \rightarrow 4f^{13}5d$ absorption transitions in the energy range below about 67000 cm^{-1} (Fig. 2-d). The features observed at higher energy but below the fundamental absorption edge are expected to represent a superposition of high-energy $4f^{14} \rightarrow 4f^{13}5d$ transitions and defect states. The latter are pronounced in the excitation spectrum for the defect emission at 27800 cm^{-1} as a broad non-uniform excitation feature spread from about 58000 to 83000 cm^{-1} with a maximum near 69500 cm^{-1} (Fig. 2-f). The peak near 71000 cm^{-1} in the Yb^{2+} excitation spectrum at T = 300 K and missing at T = 8 K (Fig. 2-d) may be connected with thermally assisted defect-to-impurity energy transfer.

The peak at 92000 cm^{-1} observed in Yb^{2+} and the defect emission excitation spectra recorded at T = 8 K are most pronounced in the excitation spectrum of STE emission (Fig. 2-g) and represents the formation of free excitons [31] as well as indicating the existence of energy transfer from STEs to Yb^{2+} and defect states. Similar to the case of $NaMgF_3:Yb^{2+}$, the STEs in MgF_2 are thermally quenched at T = 300 K thus the excitonic peak is absent in excitation spectrum recorded monitoring the Yb^{2+} $4f^{13}5d \rightarrow 4f^{14}$ emission, for this temperature. Both the Yb^{2+} and the defect emission are efficiently excited above the band gap.

The behaviour of the excitation spectra for $NaMgF_3:Yb^{2+}$ and $MgF_2:Yb^{2+}$ in the energy range of the host absorption is quite similar. At low temperature, both materials exhibit efficient energy transfer from optically excited excitons. In fluorides, free excitons typically relax into STEs characterized by a low mobility at low temperature. However, owing to their long lifetimes and the relatively high concentration of impurity ions, that increases the probability of creating excitons in the vicinity of Yb^{2+} ions, thus energy transfer via STEs becomes efficient. Reabsorption of STE emission by Yb^{2+} is also possible due to the spectral overlap of the STE emission and the lowest energetic Yb^{2+} $4f^{14} \rightarrow 4f^{13}5d$ absorption bands in both crystals. The energy transfer mechanism which occurs for above band gap excitation is likely to be more complicated. The location of the Yb^{2+} $4f^{14}$ ground state in fluorides is expected to be around 9 eV above the top of valence band (VB) [32] that excludes a direct capture of thermalized holes by Yb^{2+}. In this case, the exciton mechanism of energy transfer should obviously dominate. This is supported by the similarities in the low temperature excitation spectra when monitoring either STE, ITE or Yb^{2+} emission – for excitation above the band gap. At T = 300 K the STE emission of $NaMgF_3$ and MgF_2 is quenched as observed in our study and documented in Refs. [28,31]. The thermal quenching of STEs in fluorides is typically ascribed to thermally assisted energy transfer to neighbouring STEs (through exciton-exciton interactions) or decay into point defects like F–H pairs or Frenkel defects [33,34] – this is evident for MgF_2 [35]. This suggests that a direct energy transfer from STEs to Yb^{2+} centres, either via dipole-dipole interactions or reabsorption, should be considered as very inefficient or unlikely at T = 300 K. We suppose that under these conditions, the energy transport may be supported by elementary processes such as the relaxation of ultrashort-lived STE precursors (e.g. free excitons or polarons). The efficiency and dynamics of such processes will be dependent upon the spatial distribution of quenchers such as long lived or stationary defects and the energy of exciting photons. To get insight into this, additional experimental and theoretical studies are required. These may include a sub-ns time-resolved study of emission transients similar to that demonstrated in Ref. [36] where the dynamics of STE quenching has been considered and

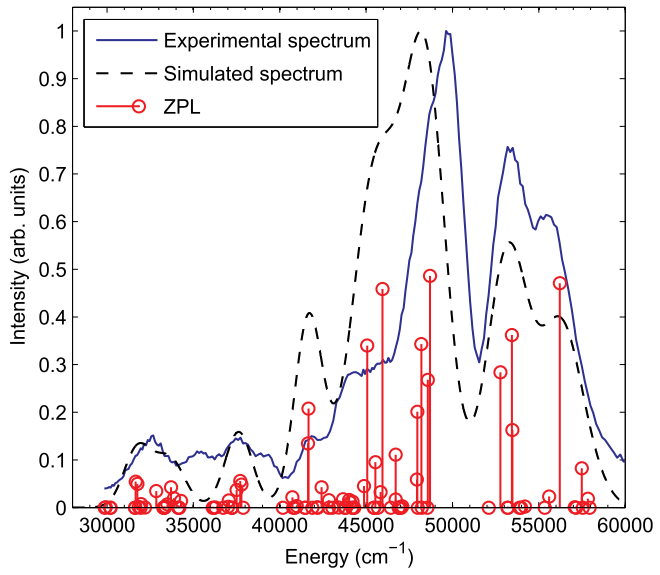

Fig. 3. Excitation spectrum of $NaMgF_3$:Yb at 8 K with λ_{em} = 25000 cm^{-1} compared to the simulated spectrum calculated with a semi-empirical crystal field model.

theoretical studies based on the modelling of processes controlled by the overlap of wave functions of the interacting states.

3.3. Crystal field models of $NaMgF_3$:Yb^{2+} and MgF_2:Yb^{2+}

The energy levels of the Yb^{2+} ion are determined using an effective (or semi-empirical) Hamiltonian, where:

$$H\psi_i = E_i\psi_i \tag{1}$$

$$H_{eff}\varphi_i = E_i\varphi_i. \tag{2}$$

The effective Hamiltonian acts on a reduced 'model space' of the full Hamiltonian consisting of only the $4f^{14}$+$4f^{13}5d$ electron configurations of the Yb^{2+} impurity. The eigenvalues of the reduced space are the same as for the full Hamiltonian, and hence the energies of these states can be calculated.

The effective Hamiltonian is constructed identically to previous work [37–39], comprising operators representing the Coulomb, spin-orbit and impurity-ligand 'crystal field' interactions, weighted by parameters that measure the magnitude of such interactions. Yb^{2+} has a ground configuration $4f^{14}$, which provides a $^1S_0$ ground state with energy $E_{avg}(f)$. In the excited configuration $4f^{13}5d$, there are no two- or three-body interactions between the $4f$ electrons. The resulting effective Hamiltonian for these $4f^{14}$+$4f^{13}5d$ states is

$$H_{4f^{13}5d} = E_{avg}(f) + \Delta_E(fd) + \zeta(f)A_{so}(f) + \sum_{k=2,4,6} B_q^k(f)C_q^{(k)}(f) + \zeta(d)A_{so}(d) + \sum_{k=2,4} F^k(fd)f_k(fd) + \sum_{j=1,3,5} G^k(fd)g_k(fd) + \sum_{k=2,4} B_q^k(d)C_q^{(k)}(d). \tag{3}$$

here $\Delta_E(fd)$ is the average energy of the $4f^{13}$ configuration relative to $4f^{14}$. The $\zeta(f)$ and $\zeta(d)$ parameters, and corresponding A_{so} operators, comprise the spin-orbit effects on the $4f$ electrons and $5d$ electron respectively. The $F^k(fd)$ and $G^k(fd)$ parameters are the direct and exchange Slater parameters for the Coulomb interaction between electrons in different shells. The B_q^k parameters describe the crystal field effects for the appropriate electrons.

Which crystal field parameters are included in the parameterised model depends on the geometry of the crystal field. In order to select relevant crystal field parameters, we must assume a structure for the

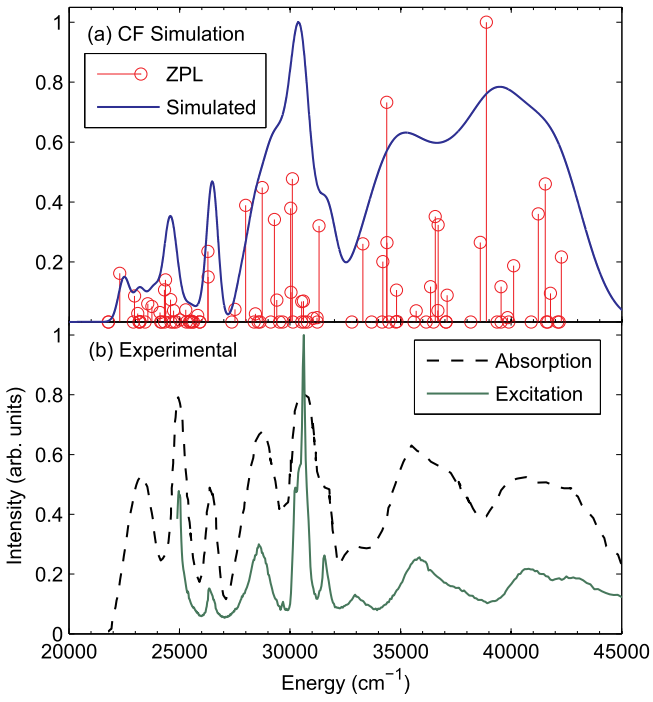

Fig. 4. (a) Simulated spectrum of MgF_2:Yb calculated with a semi-empirical crystal field model. The red lines are the zero-phonon lines (ZPLs) of the transitions and the blue line is a Gaussian convolution of the ZPLs. (b) Excitation spectrum of MgF_2:Yb at a sample temperature of 8 K with λ_{em} = 20400 cm^{-1} and the room temperature absorption spectrum reported by Kück et al. [40]. (For interpretation of the references to colour in this figure legend, the reader is referred to the Web version of this article.)

Yb^{2+} site. The Yb site symmetry was assumed to be a tetragonal distortion from octahedral symmetry for both $NaMgF_3$:Yb^{2+} and MgF_2:Yb^{2+}. The tetragonal symmetry is represented by crystal field parameters B^4 and B^6 defined such that $B_4^4 = \sqrt{\frac{15}{4}}B_0^4$ and $B_4^6 = \sqrt{\frac{7}{2}}B_0^6$. The tetragonal distortion is represented by the inclusion of a B_0^2 parameter.

Initial values for the free-ion parameters are determined from their definitions, using Hartree-Fock theory to estimate electron radial distribution functions [41]. Initial values for the crystal field parameters are taken from the CaF_2:Yb^{2+} system and reported in our previous work [5]. The direct and exchange Coulomb parameters are held fixed at the values determined by Pan et al. for $SrCl_2$:Yb^{2+} [38].

Fig. 3 shows the $4f^{14}$→$4f^{13}5d$ excitation spectrum of $NaMgF_3$:Yb^{2+} (measured at a sample temperature of 8 K) along with a simulated spectrum calculated with the semi-empirical crystal field model. The crystal field parameters were qualitatively fitted to the vacuum ultraviolet experimental spectrum.

As for $NaMgF_3$:Yb^{2+}, the $4f^{14}$→$4f^{13}5d$ transitions of MgF_2:Yb^{2+} can be approximated with a semi-empirical model of the crystal field where the site symmetry is assumed to be octahedral having a tetragonal distortion. The UV-VUV absorption spectrum (up to about 67000 cm^{-1}) of MgF_2:Yb^{2+} has been previously measured by Kück et al. [40]. The absorption spectrum has substantially different relative intensities between peaks when compared to the excitation spectrum (or fluorescence detected absorption spectrum), indicating that absorption into some Yb^{2+} $5d$ levels does not result in efficient ITE emission. Fig. 4 shows the $4f^{14}$→$4f^{13}5d$ experimental spectra for MgF_2:Yb^{2+} along with a simulated spectrum calculated with the semi-empirical crystal field model. Since the calculation models the absorption process, the crystal field parameters were qualitatively fitted to the absorption spectrum rather than the excitation spectrum. The values of the crystal field parameters are given in Table 1.

Table 1 contains the values of the crystal field parameters calculated

Table 1
Final values of parameters for the crystal field fit of Yb^{3+} in $NaMgF_3$ and MgF_2. All parameter values are given in cm^{-1}.

Parameter	Free Yb^{2+} Ion[a]	$SrCl_2$: Yb^{2+}[b]	CaF_2: Yb^{2+}[c]	$NaMgF_3$: Yb^{2+}	MgF_2: Yb^{2+}
$\Delta_E(fd)$		38832	42700	42800	42000
$\zeta(ff)$	1290	1211	1204	2000	3000
$\zeta(dd)$	2899	2950	2950	2700	1000
$F^2(fd)$	23210	14355	14355	14355[d]	14355[d]
$F^4(fd)$	10646	7222	7222	7222[d]	7222[d]
$G^1(fd)$	10059	4693	4693	4693[d]	4693[d]
$G^3(fd)$	8046	5382	5382	5382[d]	5382[d]
$G^5(fd)$	6085	4349	4349	4349[d]	4349[d]
$B_0^2(ff)$				−700	−1000
$B^4(ff)$[e]		−725	−2036	500	1000
$B^6(ff)$[f]		292	821	−200	−200
$B_0^2(dd)$[e]				−6000	8000
$B^4(dd)$[e]		−20442	−37726	22000	40000

[a] Ref [41].
[b] Ref [37].
[c] Ref [5].
[d] Not fitted here. Held at the values determined by Ref. [37].
[e] $B_0^4 = B^4$, $B_{\pm4}^4 = \sqrt{\frac{5}{14}}B^4$.
[f] $B_0^6 = B^6$, $B_{\pm4}^6 = -\sqrt{\frac{7}{2}}B^6$.

from their definitions for the free Yb^{2+} ion; those fitted to $SrCl_2$:Yb^{2+} and CaF_2:Yb^{2+} using a $4f^{14}\rightarrow4f^{13}5d$ effective Hamiltonian; and the values of parameters fitted here. The Coulomb parameters have little effect on the spectrum, and are kept at the same value for all three crystal environments. The value of the B^4 and B^6 parameters for $NaMgF_3$:Yb^{2+} are smaller than for CaF_2:Yb^{2+}.

4. Conclusion

A temperature dependent time-resolved spectroscopic study of bulk single crystals of $NaMgF_3$:Yb^{2+} and MgF_2:Yb^{2+} has been performed using UV-VUV synchrotron radiation. Emission from ITE or Yb^{2+} $4f^{13}5d$ states has been identified in the both materials. Excitation of the fundamental inter-band absorption of the respective crystals results in emission from intrinsic states and Yb^{2+} impurity centres. The interplay between intrinsic states and Yb^{2+} impurity centres is observed and analysed as a function of excitation wavelength and sample temperature.

$NaMgF_3$:Yb^{2+} was found to demonstrate similar relaxation pathways upon UV-VUV excitation to that previously published for CaF_2:Yb^{2+} [5]. However, unlike CaF_2:Yb^{2+} where the ITE and STE emission bands are separated by about 17000 cm^{-1}, in $NaMgF_3$:Yb^{2+} the emission bands from ITE and STE states noticeably overlap each other. Emission and excitation features observed for MgF_2:Yb^{2+} in the host transparency range are similar to those previously documented in Refs. [13,17,27] apart from the observation of a weak emission feature near 23400 cm^{-1} that has been tentatively assigned to a defect emission.

The lower-energy section of the excitation spectra of $NaMgF_3$:Yb^{2+} and MgF_2:Yb^{2+} are dominated by the Yb^{2+} $4f^{14}\rightarrow4f^{13}5d$ transitions. These spectra were qualitatively fitted to a semi-empirical crystal field model where the Yb^{2+} site geometry was assumed to have a tetragonal symmetry. The crystal field parameters were compared to previous work on CaF_2 and $SrCl_2$. The B^4 parameters for $NaMgF_3$:Yb^{2+} and MgF_2:Yb^{2+} have the opposite sign to CaF_2:Yb^{2+} and the magnitudes of the crystal field parameters are significantly lower for $NaMgF_3$:Yb^{2+}.

Both materials exhibit quite similar properties in terms of the host-to-Yb^{2+} energy transfer. In particular, an efficient excitonic energy transfer is observed at T = 8 K either upon excitation into the free exciton absorption band or above the band gap that is followed by the relaxation of separated e-h pairs into excitons and further to STEs. The latter may also transfer their energy via reabsorption of emission. At T = 300 K the energy transfer is likely to be driven by STE precursors; ultrashort-living electronic excitations existing within a sub-nanosecond time scale after the host excitation.

Author declaration

The authors of this manuscript have all read and agreed to the submission of this manuscript.

Declaration of competing interest

The authors declare that they have no known competing financial interests or personal relationships that could have appeared to influence the work reported in this paper.

References

[1] M.J. Weber, Inorganic scintillators: today and tomorrow, J. Lumin. 100 (2002) 35.
[2] P. Dorenbos, f→d transition energies of divalent lanthanides in inorganic compounds, J. Phys. Condens. Matter 15 (2003) 575.
[3] D.S. McClure, C. Pedrini, Excitons trapped at impurity centers in highly ionic crystals, Phys. Rev. B 32 (1985) 8465–8468.
[4] B. Moine, B. Courtois, C. Pedrini, Luminescence and photoionisation processes of Yb^{2+} in CaF_2, SrF_2 and BaF_2, J. Phys. 50 (1989) 2105.
[5] R.B. Hughes-Currie, A.J. Salkeld, K.V. Ivanovskikh, M.F. Reid, J.-P.R. Wells, R. J. Reeves, Excitons and interconfigurational transitions in CaF_2:Yb^{2+} crystals, J. Lumin. 158 (2015) 197.
[6] Z. Barandiarán, L. Seijo, Intervalence charge transfer luminescence: interplay between anomalous and 5d − 4f emissions in Yb-doped fluorite-type crystals, J. Chem. Phys. 141 (2014) 234704.
[7] Z. Barandiaran, A. Meijerink, L. Seijo, Configuration coordinate energy level diagrams of intervalence and metal-to-metal charge transfer states of dopant pairs in solids, Phys. Chem. Chem. Phys. 17 (2015) 19874–19884.
[8] R.B. Hughes-Currie, K.V. Ivanovskikh, J.-P.R. Wells, M.F. Reid, R.A. Gordon, L. Seijo, Z. Barandiarán, X-ray excitation triggers ytterbium anomalous emission in CaF_2:Yb but not in SrF_2:Yb, J. Phys. Chem. Lett. 8 (2017) 1175–1178.
[9] C. MacKeen, F. Bridges, M. Kozina, A. Mehta, M.F. Reid, J.P.R. Wells, Z. Barandiarán, Evidence that the anomalous emission from CaF_2:Yb^{2+} is not described by the impurity trapped exciton model, J. Phys. Chem. Lett. 8 (2017) 3313–3316.
[10] C. MacKeen, F. Bridges, L. Seijo, Z. Barandiarán, M. Kozina, A. Mehta, M.F. Reid, J. P.R. Wells, The complexity of the CaF_2:Yb system: a huge, reversible, X-ray-induced valence reduction, J. Phys. Chem. C 121 (2017) 28435–28442.
[11] C. Dotzler, G.V.M. Williams, U. Reiser, A. Edgar, Optically stimulated luminescence in $NaMgF_3$:Eu^{3+} crystals, Appl. Phys. Lett. 91 (2007) 121910.
[12] N. Le Masson, A. Box, C. van Eijk, C. Furetta, J.-P. Chaminade, Optically and thermally stimulated luminescence of $KMgF_3$:Ce^{3+} and $NaMgF_3$:Ce^{3+}, Radiat. Prot. Dosim. 100 (2002) 229.
[13] S. Lizzo, A. Meijerink, G. Dirkson, G. Blasse, On the luminescence of divalent ytterbium in $KMgF_3$ and $NaMgF_3$, J. Phys. Chem. Solids 56 (1995) 959.
[14] R.B. Hughes-Currie, P.S. Senanayake, J.-P.R. Wells, M.F. Reid, G. Berden, R. J. Reeves, A. Meijerink, Site selective transient photoluminescence enhancement of impurity trapped excitons in $NaMgF_3$:Yb^{2+}, Phys. Rev. B. 88 (2013) 104304.
[15] S. Lizzo, A. Meijerink, G. Dirkson, G. Blasse, Luminescence of divalent ytterbium in magnesium fluoride crystals, J. Lumin. 63 (1995) 223.
[16] P. Dorenbos, Anomalous luminescence of Eu^{2+} and Yb^{2+} in inorganic compounds, J. Phys. Condens. Matter 15 (2003) 2645.
[17] P.S. Senanayake, J.-P.R. Wells, M.F. Reid, G. Berden, A. Meijerink, R.J. Reeves, Electron trap liberation in MgF_2 doped with Yb^{2+} using a color excitation experiment, Appl. Phys. Lett. 100 (2012) 041902.
[18] M.F. Reid, P.S. Senanayake, J.-P.R. Wells, G. Berden, A. Meijerink, A.J. Salkeld, C.-K. Duan, R.J. Reeves, Transient photoluminescence enhancement as a probe of the structure of impurity trapped excitons in CaF_2:Yb^{2+}, Phys. Rev. B. 84 (2011) 113110.
[19] E. Van der Kolk, P. Dorenbos, C.W.E. van Eijk, A.P. Vink, M. Weil, J.P. Chaminade, Luminescence excitation study of higher energy states of Pr^{3+} and Mn^{2+} in $SrAlF_5$, $CaAlF_5$ and $NaMgF_3$, J. Appl. Phys. 95 (2004) 7867.
[20] R.B. Hughes-Currie, K.V. Ivanovskikh, J.-P.R. Wells, M.F. Reid, R.A. Gordon, The determination of dopant ion valence contributions in insulating crystals using XANES measurements, J. Phys. Condens. Matter 28 (2016) 135502.
[21] G. Zimmerer, SUPERLUMI: a unique set up for luminescence spectroscopy with synchrotron radiation, Radiat. Meas. 42 (2007) 859.
[22] H. Takahashi, R. Onaka, The XUV spectra of $KMgF_3$ and $NaMgF_3$, J. Phys. Soc. Jpn. 43 (1977) 2021.
[23] A.N. Belsky, J. Krupa, Luminescence excitation mechanisms of rare-earth doped phosphors in the VUV range, Displays 19 (1999) 185.

[24] Y. Zhou, S.P. Feofilov, H.J. Seo, J.Y. Jeong, D.A. Keszler, R.S. Meltzer, Energy transfer to Gd^{3+} from the self-trapped exciton in $ScPO_4:Gd^{3+}$: dynamics and applications to quantum cutting, Phys. Rev. B. 77 (2008) 075129.
[25] R.T. Williams, K.S. Song, The self-trapped exciton, J. Phys. Chem. Solids 51 (1990) 679.
[26] V.V. Mikhailin, Excitation of secondary processes in the vacuum ultraviolet range, Nucl. Instrum. Methods Phys. Res. A. 261 (1987) 107.
[27] I.A. Kamenskikh, V.V. Mikhailin, I.N. Shpinkov, A.N. Vasil'yev, High-energy excitation of luminescence of crystals with oxyanions, Nucl. Instrum. Methods Phys. Res. A. 282 (1989) 599.
[28] D. Wisniewski, L.A. Boatner, Scintillation properties and time-resolved spectroscopy of a novel scintillator material: Ce^{3+}-activated $Li_3Lu(PO4)_2$ crystals, nuclear science, IEEE Transactions on 56 (2009) 3806–3818.
[29] A.S. Voloshinovskii, V.B. Mikhailik, P.A. Rodnyi, Luminescence of on- and off-center STE in ABX_3 crystals, Radiat. Eff. Defects Solids 135 (1995) 281.
[30] O.E. Facey, W.A. Silbey, M centers in MgF_2 crystals, Phys. Rev. B. 2 (1970) 1111.
[31] V. Kolobanov, V. Mikhailin, C. Chernov, D. Spassky, V. Makhov, M. Kirm, E. Feldbach, S. Vielhauer, Luminescence of singlet self-trapped excitons in MgF_2, J. Phys. Condens. Matter 21 (2009) 375501.
[32] P. Dorenbos, Locating lanthanide impurity levels in the forbidden band of host crystals, J. Lumin. 108 (2004) 301.
[33] K. Kimura, W. Hong, Decay enhancement of self-trapped excitons at high density and low temperature in an ion-irradiated BaF2 single crystal, Phys. Rev. B. 58 (1998) 6081.
[34] E.A. Kotomin, A.I. Popov, The kinetics of radiation-induced point defect aggregation and metallic colloid formation in ionic solids, in: K.E. Sickafus, E. A. Kotomin, B.P. Uberuaga (Eds.), Radiation Effects in Solids, Springer Netherlands, Dordrecht, 2007, pp. 153–192.
[35] V.M. Lisitsyn, L.A. Lisitsyna, A.I. Popov, E.A. Kotomin, F.U. Abuova, A. Akilbekov, J. Maier, Stabilization of primary mobile radiation defects in MgF_2 crystals, Nucl. Instrum. Methods B. 374 (2016) 24.
[36] N. Fedorov, A. Belsky, E. Constant, D. Descamps, P. Martin, A.N. Vasil'ev, Quenching of excitonic luminescence of alkaline earth fluorides excited by VUV harmonics of femtosecond laser, J. Lumin. 129 (2009) 1813.
[37] A.J. Salkeld, M.F. Reid, J.-P.R. Wells, G. Sánchez-Sanz, L. Seijo, Z. Barandiarán, Effective Hamiltonian parameters for ab initio energy-level calculations of $SrCl_2:Yb^{2+}$ and $CsCaBr_3:Yb^{2+}$, J. Phys. Condens. Matter 25 (2013) 415504.
[38] Z. Pan, C.-K. Duan, P.A. Tanner, Electronic spectra and crystal-field analysis of Yb^{2+} in $SrCl_2$, Phys. Rev. B. 77 (2008), 085114.
[39] G.W. Burdick, M.F. Reid, in: K.A. Gsneidner Jr., J.C. Bunzli, V.K. Percharsky (Eds.), Handbook on the Physics and Chemistry of the Rare Earths, vol.37, North Holland, 2007, pp. 61–91. Ch 232.
[40] S. Kück, M. Henke, K. Rademaker, Crystal growth and spectroscopic investigation of Yb^{2+}-doped fluoride crystals, Laser Phys. 11 (2001) 116–119.
[41] R.D. Cowan, The Theory of Atomic Structure and Spectra, vol. 3, University of California Press, 1981.